

Enhanced low-field magnetocaloric effect induced by Co doping in RCu$_{2-x}$Co$_x$ (R = Er, Ho) compounds for liquid hydrogen

Lu Tian(田路), Zhaojun Mo(莫兆军), Xuanyu Qiao(乔轩雨), Chenyang Ma(马辰洋), and Guodong Liu(刘国栋)
Citation: Chin. Phys. B, 2026, 35 (**7**): 077505. DOI: 10.1088/1674-1056/ae360a
http://cpb.iphy.ac.cn; http://iopscience.iop.org/cpb

What follows is a list of articles you may be interested in

Strain energy enhanced room-temperature magnetocaloric effect in Mn_5Ge_3

Xiaohe Liu(刘潇贺), Ping Song(宋平), Sen Yao(姚森), Yuhao Lei(雷雨豪), Ling Yang(杨玲), Shenxiang Du(杜深祥), Yiran Deng(邓贻然), and Defeng Guo(郭得峰)
Chin. Phys. B, 2026, 35 (**2**): 027505. DOI: 10.1088/1674-1056/adf6a6

Tuning the magnetocaloric and structural properties of $La_{0.67}Sr_{0.28}Pr_{0.05}Mn_{1-x}Co_xO_3$ refrigeration materials

Changji Xu(徐长吉), Xinyu Jiang(姜心雨), Zhengguang Zou(邹正光), Zhuojia Xie(谢卓家), Weijian Zhang(张伟建), and Min Feng(冯敏)
Chin. Phys. B, 2024, 33 (**12**): 127501. DOI: 10.1088/1674-1056/ad8550

Magnetic and magnetocaloric effect of $Er_{20}Ho_{20}Dy_{20}Cu_{20}Ni_{20}$ high-entropy metallic glass

Shi-Lin Yu(于世霖), Lu Tian(田路), Jun-Feng Wang(王俊峰), Xin-Guo Zhao(赵新国), Da Li(李达), Zhao-Jun Mo(莫兆军), and Bing Li(李昺)
Chin. Phys. B, 2024, 33 (**5**): 057502. DOI: 10.1088/1674-1056/ad1a94

Mechanical and magnetocaloric adjustable properties of Fe_3O_4/PET deformed nanoparticle film

Fengguo Fan(范凤国) and Lintong Duan(段林彤)
Chin. Phys. B, 2024, 33 (**3**): 037502. DOI: 10.1088/1674-1056/acf280

Giant low-field cryogenic magnetocaloric effect in polycrystalline $LiErF_4$ compound

Zhaojun Mo(莫兆军), Jianjian Gong(巩建建), Huicai Xie(谢慧财), Lei Zhang(张磊), Qi Fu(付琪), Xinqiang Gao(高新强), Zhenxing Li(李振兴), and Jun Shen(沈俊)
Chin. Phys. B, 2023, 32 (**2**): 027503. DOI: 10.1088/1674-1056/ac65ef

---

SPECIAL TOPIC — Multiferroicity and multicaloric effects

Enhanced low-field magnetocaloric effect induced by Co doping in $R\mathrm{Cu}_{2-x}\mathrm{Co}_x$ (R = Er, Ho) compounds for liquid hydrogen

Lu Tian(田路)[1], Zhaojun Mo(莫兆军)[1,†], Xuanyu Qiao(乔轩雨)[1], Chenyang Ma(马辰洋)[2], and Guodong Liu(刘国栋)[2]

[1] *Key Laboratory of Rare Earths, Ganjiang Innovation Academy, Chinese Academy of Sciences, Ganzhou* 341000, *China*
[2] *School of Science, Hebei University of Technology, Tianjin* 300130, *China*

(Received 21 November 2025; revised manuscript received 6 January 2026; accepted manuscript online 9 January 2026)

Hydrogen, as a clean energy carrier, requires liquefaction at 20–77 K, a process that is energy-intensive and traditionally dependent on conventional refrigeration methods. Magnetocaloric refrigeration offers a promising alternative, especially when using permanent magnets as the magnetic field source, which can significantly simplify system design and reduce operational costs. Designing magnetocaloric materials with magnetic ordering temperatures within the hydrogen liquefaction range and exhibiting superior magnetocaloric effects under low magnetic fields is essential for advancing sustainable energy technologies. This study presents an in-depth investigation of the enhanced low-field magnetocaloric effect (MCE) in $R\mathrm{Cu}_{2-x}\mathrm{Co}_x$ (R = rare-earth) compounds. The results indicate that Co doping significantly modifies orbital hybridization and magnetic properties, which in turn improves the MCE under low fields. Experimental data confirm that Co-doped compounds show MCE performance at low fields. For instance, under a varying magnetic field of 0–2 T, the volumetric magnetic entropy change of the $\mathrm{ErCu}_{1.75}\mathrm{Co}_{0.25}$ compound reaches 0.12 J·cm^{-3}·K^{-1}. First-principles calculations provide further insights into the electronic density of states and magnetic exchange interactions, clarifying the mechanisms behind the enhanced MCE.

Keywords: magnetocaloric effect, hydrogen liquefaction, low magnetic fields, first-principles calculations

PACS: 75.30.Sg, 75.47.Pq

DOI: 10.1088/1674-1056/ae360a **CSTR:** 32038.14.CPB.ae360a

1. Introduction

Utilizing hydrogen as a new energy carrier is one of the key approaches to achieving the goals of pollution-free and highly efficient sustainable energy.[1] Hydrogen's potential lies not only in its abundance but also in its ability to store and release energy without producing harmful by-products.[2,3] However, the liquefaction of hydrogen, a critical step for its storage and transportation, remains an energy-intensive process that typically requires temperatures below 20 K. Traditional hydrogen liquefaction processes are characterized by high energy consumption and require complex system configurations.[4] Magnetocaloric refrigeration, offering an alternative that leverages the magnetocaloric effect (MCE), has garnered attention due to its potential to simplify the liquefaction process while reducing energy consumption, particularly when materials are optimized to exhibit significant MCE.[5–8]

Rare-earth (RE)-based compounds are fertile ground for developing magnetocaloric materials due to their intrinsic large magnetic moments.[9–13] However, RE-based compounds often exhibit antiferromagnetic interactions due to the influences of electronic structure, localization effects, exchange interactions, and crystal field effects, which typically lead to suboptimal magnetocaloric effects in low magnetic fields.[14–17] Regulating the magnetic interactions of rare-earth-based compounds towards a ferromagnetic state to achieve significant magnetocaloric effects in low magnetic fields is a key challenge and focus of magnetic refrigeration (MR) applications for hydrogen liquefaction.[18,19] Hao *et al.*[20] reported that the dual-field application of pressure and magnetic field can significantly enhance the magnetocaloric effect of HoCuSi compounds in low magnetic fields. Xie *et al.*[21] found that doping elements into $EuTiO_3$-based compounds induces a shift in magnetic interactions to a ferromagnetic state due to changes in lattice constants and electronic structure, leading to a significant enhancement of the MCE. Therefore, many potential rare-earth-based compounds that exhibit a significant magnetocaloric effect in low magnetic fields merit further in-depth investigation.

Orthorhombic-type $R\mathrm{Cu}_2$ (R = rare-earth) compounds have garnered widespread interest due to their intriguing magnetism.[22–26] Although this series of compounds exhibits high saturation magnetization, their MCE performance in low fields is suboptimal due to antiferromagnetic interactions. Controlling the magnetic interactions to enhance their MCE under low fields is crucial for practical applications but remains a challenge. For transition metals, the magnetic moment is generated by the unequal number of electrons with oppo-

†Corresponding author. E-mail: mozhaojun@gia.cas.cn

© 2026 Chinese Physical Society and IOP Publishing Ltd. All rights, including for text and data mining, AI training, and similar technologies, are reserved.

site spins, caused by the strong Coulomb repulsion between their 3d electrons.[27] Thus, incorporating transition metals into rare-earth-based compounds offers the potential to modulate magnetic interactions and observe intriguing magnetic behaviors.

In this work, we systematically investigate the magnetic and magnetocaloric properties of $R\mathrm{Cu}_{2-x}\mathrm{Co}_x$ (R = Er, Ho) compounds, with a focus on understanding how Co substitution modulates magnetic interactions and enhances low-field MCE performance. Through a combination of magnetization and specific heat measurements, together with first-principles density functional theory calculations, we elucidate the role of Co in transforming the magnetic ground state and improving magnetocaloric efficiency under low magnetic fields. The results provide valuable insights into the electronic and magnetic mechanisms that govern MCE in rare-earth intermetallics, offering design principles for developing high-performance magnetocaloric materials suited for hydrogen liquefaction applications.

2. Experimental details

Polycrystalline $R\mathrm{Cu}_{2-x}\mathrm{Co}_x$ alloys were prepared via a standard arc-melting protocol under inert argon gas protection. Metallic precursors (R, Cu, Co) with certified purity $> 99.9\%$ underwent four successive melting cycles to achieve compositional uniformity, with intermediate ingot rotation during each remelting step. Subsequent homogenization annealing was performed at 1023 K for 21 days in evacuated quartz ampoules, followed by rapid quenching in an ice-water bath. Room-temperature phase identification was conducted via powder x-ray diffractometry employing Cu $K\alpha$ radiation ($\lambda = 1.5406$ Å). Magnetic properties were evaluated using two complementary techniques: (i) superconducting quantum interference device (SQUID) magnetometry and (ii) vibrating sample magnetometry (VSM), both integrated within a Quantum Design PPMS-9 cryogenic platform.

Electronic structure calculations were implemented through the Vienna ab initio simulation package (VASP) employing density functional theory (DFT) formalism.[28] Exchange–correlation effects were treated via the Perdew–Burke–Ernzerhof generalized gradient approximation (PBE–GGA).[29,30] Geometric optimization and electronic self-consistency procedures utilized a plane-wave cutoff energy of 450 eV and Γ-centered $7 \times 5 \times 3$ k-mesh sampling. Iterative convergence criteria required total energy fluctuations below 10^{-6} eV between successive cycles. On-site Coulomb interactions were incorporated through the Hubbard U correction ($U = 3$ eV) for transition d and f orbitals. Post-processing analysis including density of states (DOS) decomposition was executed via the Vaspkit toolkit.[31]

3. Results and discussion

The crystal structures of $R\mathrm{Cu}_{2-x}\mathrm{Co}_x$ (R = Er, Ho) compounds at room temperature were determined using powder x-ray diffraction (XRD) with a Cu-$K\alpha$ target, with the refined patterns shown in Figs. 1(a)–1(d). This series of compounds crystallizes in an orthorhombic structure, corresponding to space group *Imma* (No. 74). No formation of new compounds involving R, Cu, and Co was observed after doping, indicating that the structural symmetry remains unchanged upon Co substitution. The refined crystal structure information is listed in Table 1. Additionally, refinement reveals the presence of minor R_2O_3 impurities in the series of compounds. The respective contents are 2.34 wt%, 2.87 wt%, 2.75 wt%, and 4.15 wt% in the $\mathrm{ErCu}_{1.75}\mathrm{Co}_{0.25}$, $\mathrm{ErCu}_{1.5}\mathrm{Co}_{0.5}$, $\mathrm{HoCu}_{1.75}\mathrm{Co}_{0.25}$, and $\mathrm{HoCu}_{1.5}\mathrm{Co}_{0.5}$ compounds, respectively.

Table 1. Crystal structure information of $R\mathrm{Cu}_{2-x}\mathrm{Co}_x$ compounds after refinement.

Parameters		$\mathrm{ErCu}_{1.75}\mathrm{Co}_{0.25}$	$\mathrm{ErCu}_{1.5}\mathrm{Co}_{0.5}$	$\mathrm{HoCu}_{1.75}\mathrm{Co}_{0.25}$	$\mathrm{HoCu}_{1.5}\mathrm{Co}_{0.5}$
a (Å)		4.258(3)	4.245(8)	4.267(4)	4.260(7)
b (Å)		6.763(5)	6.788(5)	6.796(2)	6.773(3)
c (Å)		7.253 (4)	7.235(2)	7.262(6)	7.267(6)
V (Å^3)		208.863	208.476	210.587	209.674
R^{3+} (x, y, z)	4e	(1/2, 1/4, 0.044)			
Cu (Co) (x, y, z)	8h	(1/2, 0.448, 0.664)			
Impurity (wt%)	R_2O_3	2.34	2.87	2.75	4.15
R_p (%)		6.265	7.824	6.233	7.779
R_{wp} (%)		8.096	10.231	8.001	10.353
R_F (%)		1.333	1.805	1.231	1.859

Figures 2(a)–2(d) illustrate schematic representations of the crystal structures of compounds $R\mathrm{Cu}_{2-x}\mathrm{Co}_x$ (R = Er, Ho) from different perspectives, as well as the local environment of R^{3+} ions. In this structure, R and Cu/Co occupy the Wyckoff positions 4e and 8h, respectively. Each R^{3+} ion forms a tetrahedral coordination with six neighboring Cu/Co atoms. The adjacent tetrahedra share edges but do not share vertices. To further determine the composition of $R\mathrm{Cu}_{2-x}\mathrm{Co}_x$ (R = Er, Ho) compounds, the microstructure and elemental distribution of this series of compounds were analyzed as shown in

Figs. 3(a)–3(d). Overall, the surface of the samples appears uniform, with only some R_2O_3 impurities observable and no other phases present. Based on energy dispersive spectroscopy (EDS), the average atomic ratios of R, Cu, and Co were determined, and the results confirm that all samples are consistent with their nominal chemical compositions.

The magnetic susceptibility of $RCu_{2-x}Co_x$ (R = Er, Ho) compounds was measured as a function of temperature under a magnetic field of 0.05 T, as illustrated in Figs. 4(a)–4(d). All compounds exhibited characteristics of ferromagnetic behavior at low temperatures, indicating that the substitution of Co significantly alters the magnetic properties. The dM/dT curves reveal two magnetic ordering transitions within $RCu_{2-x}Co_x$ (R = Er, Ho) compounds, designated as T_{c1} and T_{c2} for the magnetic transition temperatures of R^{3+} and Co^{2+}, respectively. The T_{c1} values for $ErCu_{1.75}Co_{0.25}$, $ErCu_{1.5}Co_{0.5}$, $HoCu_{1.75}Co_{0.25}$, and $HoCu_{1.5}Co_{0.5}$ compounds are 14 K, 13.3 K, 16.5 K, and 17.3 K, and the corresponding T_{c2} values are 83 K, 78.9 K, 130.8 K, and 121.7 K, respectively. The inverse magnetic susceptibility curves ($1/\chi = H/M$) were analyzed based on the Curie–Weiss law,

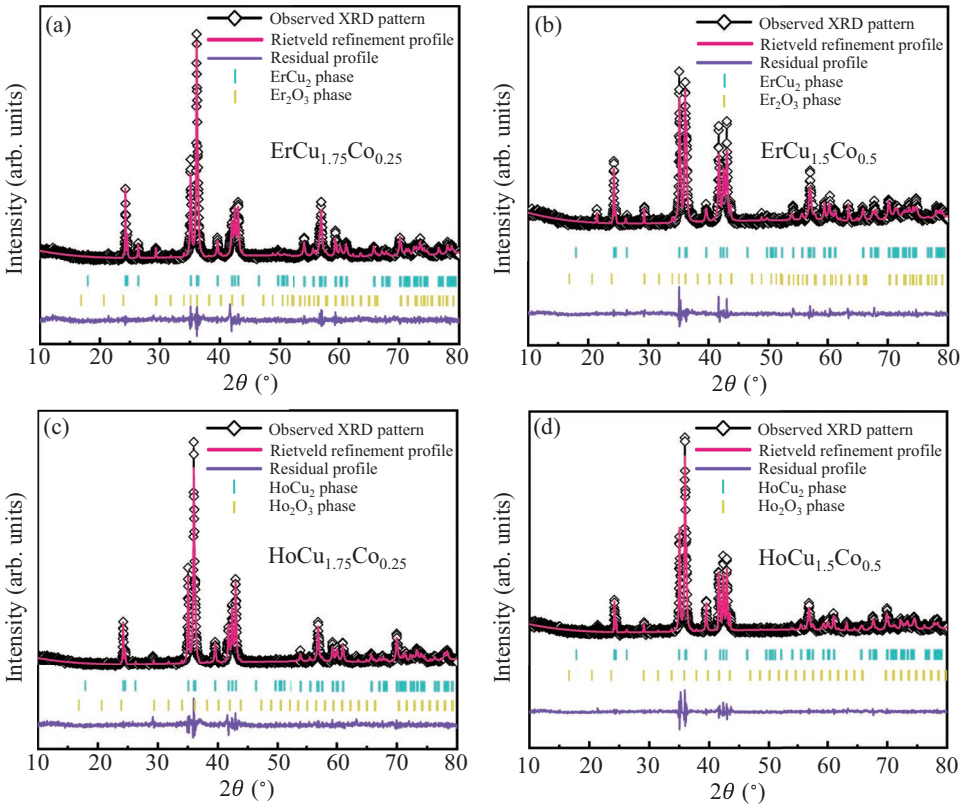


Fig. 1. (a)–(d) The room-temperature XRD patterns after refinement are presented. The green and yellow vertical lines represent the standard peak positions of the RCu_2 and R_2O_3 phases, respectively.

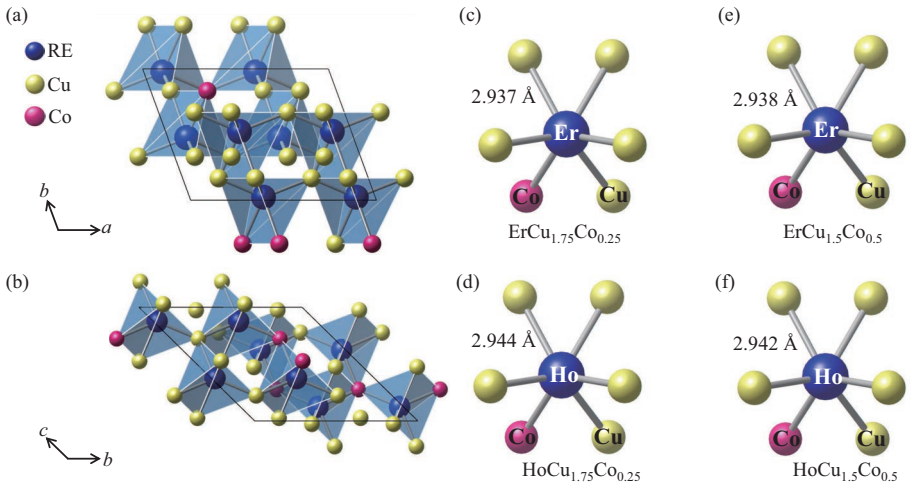


Fig. 2. (a) and (b) Schematic illustrations of the crystal structures from different perspectives. (c)–(f) The atomic environments of R^{3+} at various Co doping levels are depicted.

with experimental values represented by blue circles and fitted values by solid red lines in the figure. The fitted paramagnetic Curie temperatures were found to be 16.6 K, 33.1 K, 27.4 K, and 53.2 K, situated between T_{c1} and T_{c2}. The effective magnetic moments ($\mu_{\rm eff}^{\rm exp}$) for these compounds were slightly below the theoretical values, recorded as 9.56 $\mu_{\rm B}$, 9.16 $\mu_{\rm B}$, 10.30 $\mu_{\rm B}$, and 9.94 $\mu_{\rm B}$. Given these results, the current interpretation appears insufficient. Subsequently, results of theoretical calculations were employed to gain further insights into the magnetic interactions and electronic structure of this series of compounds.

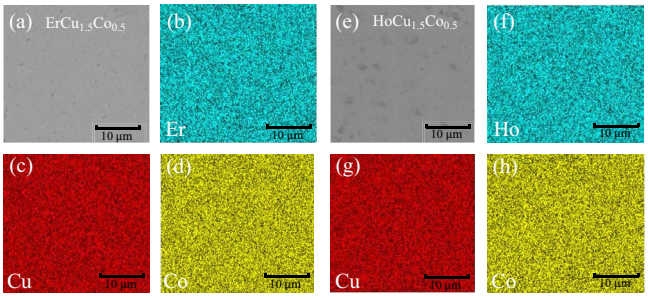


Fig. 3. Scanning electron microscope images of $ErCu_{1.5}Co_{0.5}$ and $HoCu_{1.5}Co_{0.5}$ compounds, along with the corresponding elemental distributions.

The $M(T)$ curve results indicate that the magnetic interactions in this series of compounds are ferromagnetic. The unclear aspect is the magnetic interaction between Co^{2+} and R^{3+}. Therefore, the magnetic structures of $RCu_{2-x}Co_x$ (R = Er, Ho) compounds were first determined. By calculating the free energy under different magnetic configurations, it was found that the magnetic configuration of these compounds is such that R^{3+} and Co^{2+} individually exhibit ferromagnetic ordering, whereas the interaction between these magnetic ions is antiferromagnetic. Subsequently, the DOS in both spin directions for $RCu_{2-x}Co_x$ (R = Er, Ho) compounds was calculated, as shown in Figs. 5(a)–5(d). In all compounds, the DOS for R^{3+} and Co^{2+} shows significant differentiation, exhibiting typical ferromagnetic characteristics. Moreover, as the Co content increases, the differentiation for Co^{2+} becomes more pronounced. The clarified points are as follows: (i) Both R^{3+} and Co^{2+} exhibit ferromagnetic ordering, but their magnetic moments are antiferromagnetically aligned. (ii) Higher Co^{2+} doping leads to more pronounced magnetic anomalies at higher temperatures. (iii) Co doping significantly alters the electronic structure, driving the emergence of the ferromagnetic state in R^{3+}. Due to the antiferromagnetic coupling between Co^{2+} and R^{3+}, the paramagnetic Curie temperature lies between T_{c1} and T_{c2}, and the $\mu_{\rm eff}^{\rm exp}$ is smaller than the theoretical effective magnetic moment ($\mu_{\rm eff}^{\rm th}$). The charge density projections along the c-axis for $ErCu_{1.5}Co_{0.5}$ and $HoCu_{1.5}Co_{0.5}$ are presented in Figs. 6(a) and 6(b). There is a substantial amount of localized charge around R^{3+}, indicating that R^{3+} contributes a significant magnetic moment. However, it is evident that there is a small amount

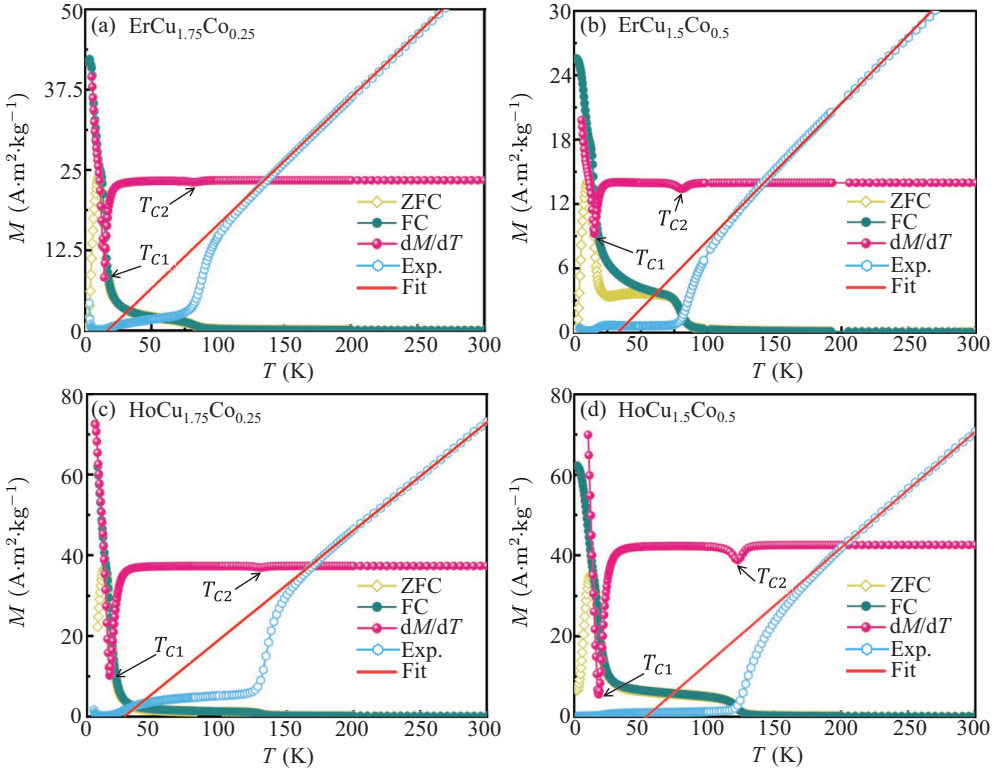


Fig. 4. (a)–(d) Temperature-dependent magnetic susceptibility curves $M(T)$ under a 0.05 T magnetic field. The pink curve represents the dM/dT curve. Blue and red lines indicate the experimental and fitted values based on the Curie–Weiss law, respectively. The black arrows point to T_{c1} and T_{c2}, which represent the Curie temperatures associated with R^{3+} and Co^{2+}, respectively.

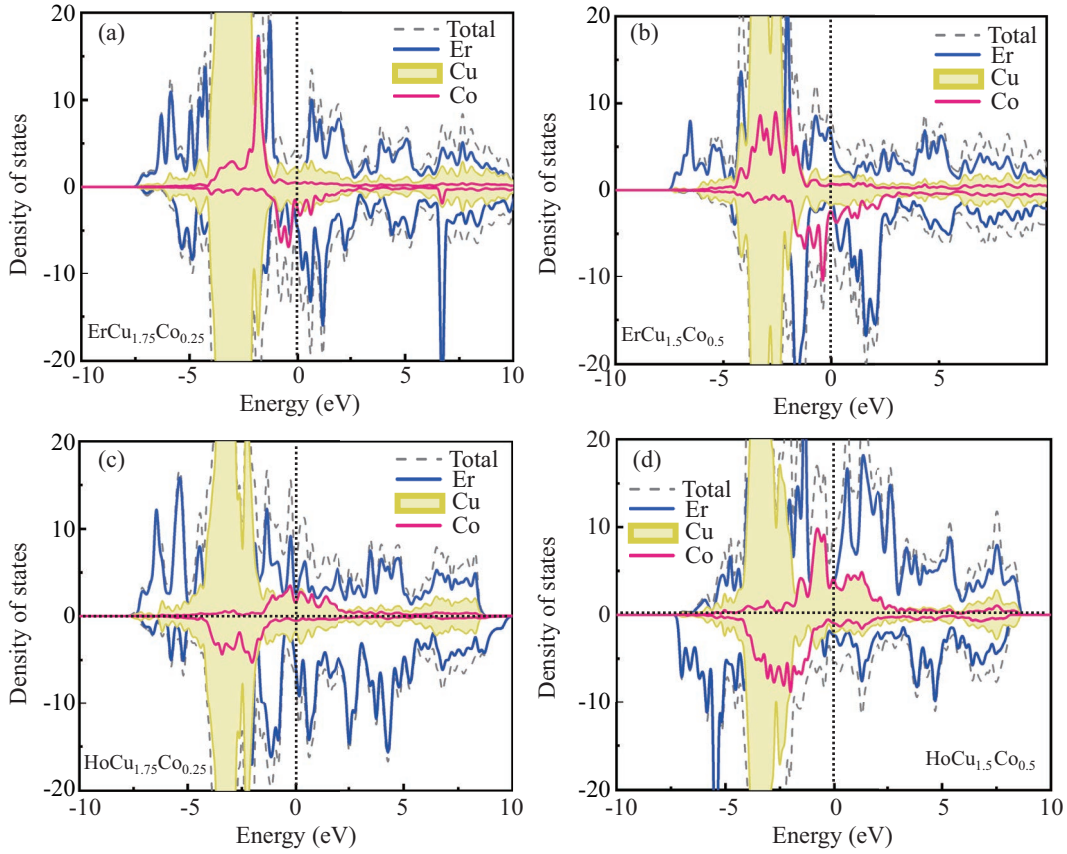


Fig. 5. DOS for different elements in both spin-up and spin-down configurations.

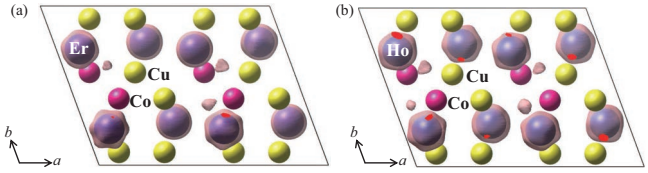


Fig. 6. (a) and (b) Two-dimensional charge density projections along the c-axis for $ErCu_{1.5}Co_{0.5}$ and $HoCu_{1.5}Co_{0.5}$ compounds.

of charge between the R and Co elements, further indicating that Co^{2+} is magnetic and undergoes strong orbital exchange interactions with R^{3+}.

To further understand the magnetism of $RCu_{2-x}Co_x$ (R = Er, Ho) compounds under magnetic fields, isothermal magnetization curves $M(H)$ at different temperatures were measured within a 0–5 T field range, as shown in Figs. 7(a)–7(d). The magnetization of all compounds sharply increases with the magnetic field and saturates around 1 T, exhibiting typical ferromagnetic characteristics. Notably, the $ErCu_{1.75}Co_{0.25}$ compound reaches a saturation magnetization as high as 154 $A{\cdot}m^2{\cdot}kg^{-1}$, indicating an excellent magnetocaloric effect (MCE), particularly pronounced at low fields. Additionally, the magnetization curves of all compounds at high temperatures do not show linear paramagnetic behavior but instead increase initially before becoming linear. This is due to the magnetic ordering of Co^{2+}, consistent with the experimental results and theoretical predictions.

The type of magnetic phase transition (MPT) in magnetic materials significantly affects their MCE performance. Arrott plots (H/M vs. M^2), derived from the transformation of $M(H)$ curves based on the Banerjee criterion, can be used to determine the order of the MPT.[32] Typically, a negative slope in an Arrott plot indicates a first-order magnetic phase transition, while a positive slope suggests a second-order transition. The Arrott plots for $RCu_{2-x}Co_x$ (R = Er, Ho) compounds are shown in Figs. 8(a)–8(d). The results indicate that all compounds undergo a second-order magnetic phase transition from the FM to the PM state.

Next, we focus on the MCEs of $RCu_{2-x}Co_x$ (R = Er, Ho) compounds. Generally, the MCE can be evaluated by approximating the temperature-dependent magnetic entropy change curve $-\Delta S_M(T)$ using the Maxwell thermodynamic relation[33]

$$\begin{aligned} -\Delta S_M &= S_M(T,0) - S_M(T,H) \\ &= -\int_0^{H_{\max}} \left(\frac{\partial M(T,H)}{\partial T}\right) \mathrm{d}H. \end{aligned} \tag{1}$$

The $-\Delta S_M(T)$ for $RCu_{2-x}Co_x$ (R = Er, Ho) compounds under different magnetic fields were calculated, as shown in Figs. 9(a)–9(d). For all compounds, the temperature corresponding to the maximum magnetic entropy change ($-\Delta S_M^{\max}$) increases with the applied magnetic field, which

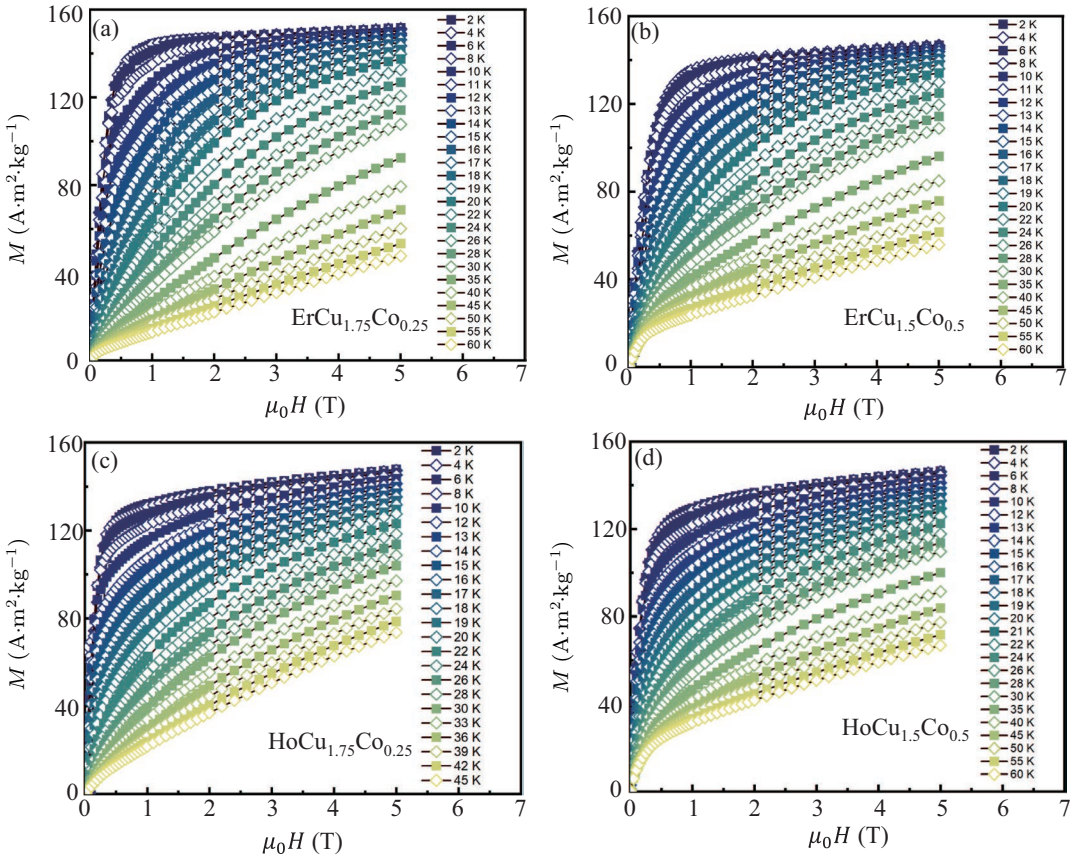


Fig. 7. (a)–(d) Isothermal magnetization curves $M(H)$ measured at different temperatures under magnetic fields ranging from 0 to 5 T.

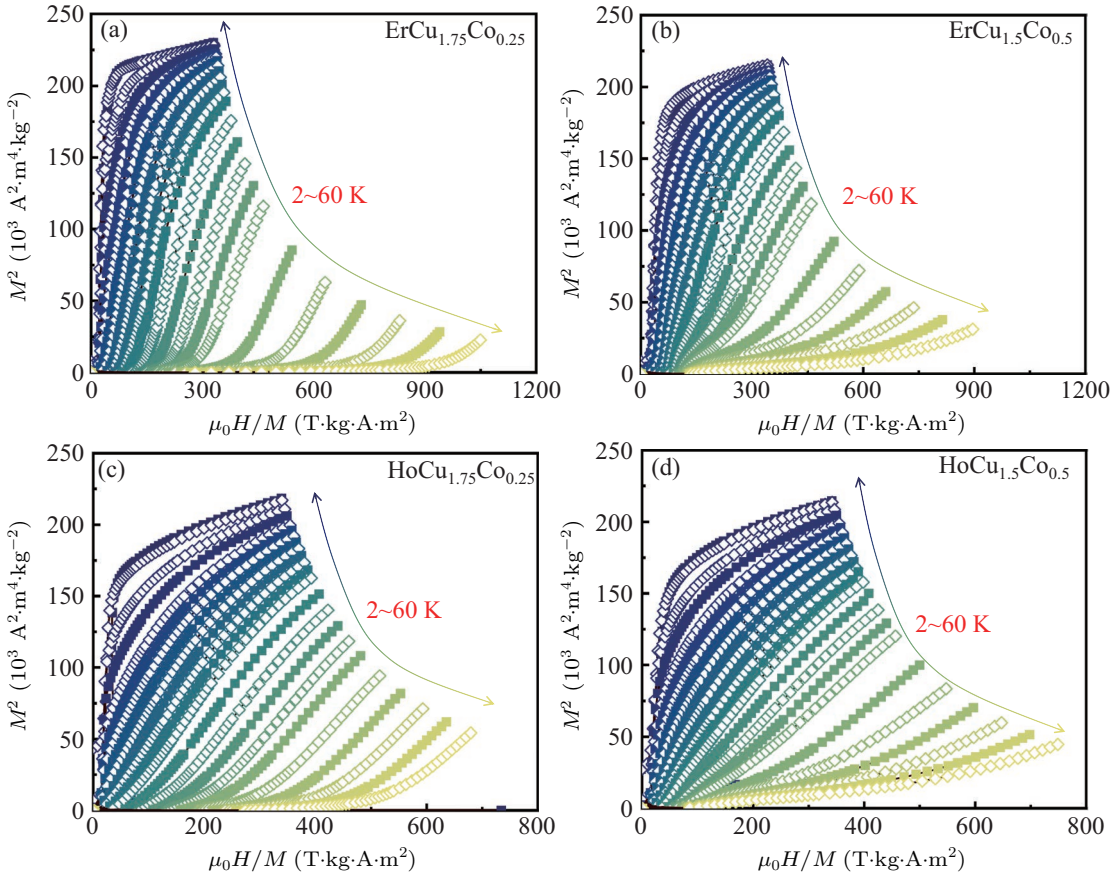


Fig. 8. (a)–(d) Arrott plots (M^2 vs. $\mu_0 H/M$) at different temperatures.

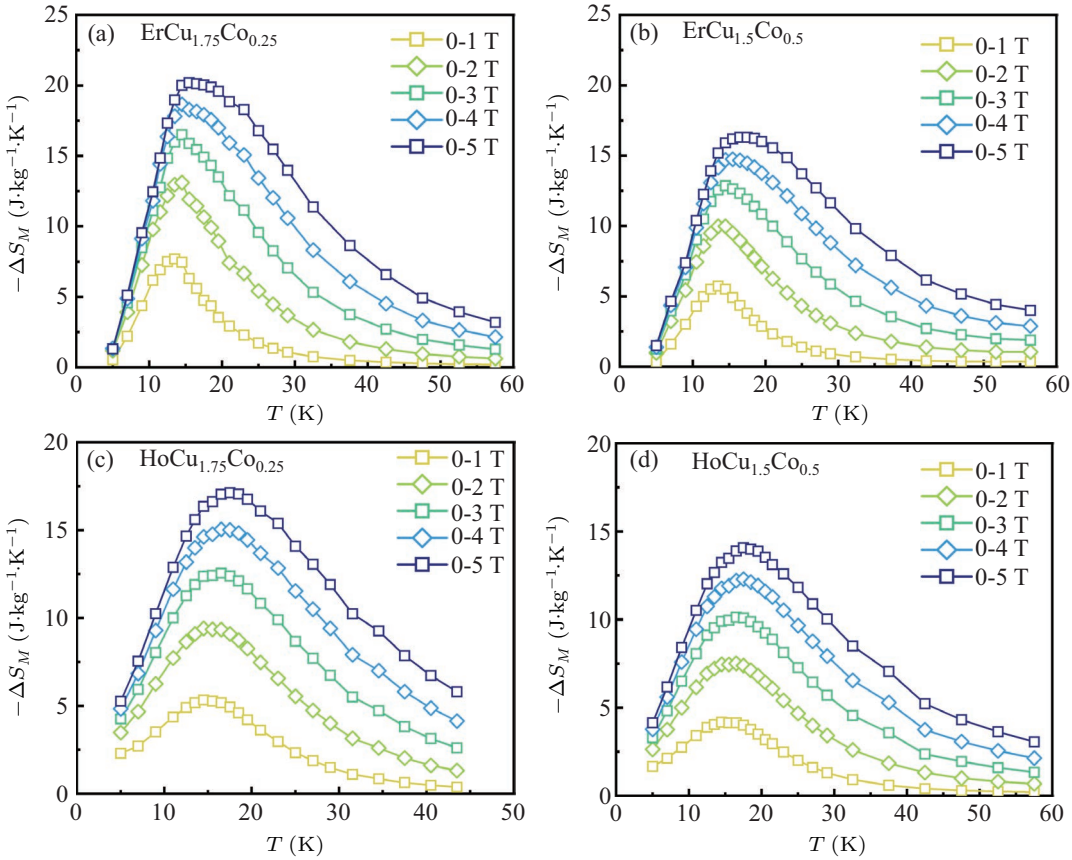


Fig. 9. Temperature dependence of the magnetic entropy change $-\Delta S_M(T)$ under varying magnetic fields of 0–5 T.

is a typical characteristic of ferromagnetic materials. Under a changing magnetic field of 0–2 T, the $-\Delta S_M^{\max}$ for $ErCu_{1.75}Co_{0.25}$, $ErCu_{1.5}Co_{0.5}$, $HoCu_{1.75}Co_{0.25}$, and $HoCu_{1.5}Co_{0.5}$ compounds are 13.1 $J{\cdot}kg^{-1}{\cdot}K^{-1}$, 9.9 $J{\cdot}kg^{-1}{\cdot}K^{-1}$, 9.4 $J{\cdot}kg^{-1}{\cdot}K^{-1}$, and 7.5 $J{\cdot}kg^{-1}{\cdot}K^{-1}$, respectively. It is worth noting that the study by Rajivgandhi *et al.*[27] indicates that the $-\Delta S_M^{\max}$ for $ErCu_2$ and $HoCu_2$ compounds under a changing magnetic field of 0–2 T are 2.5 $J{\cdot}kg^{-1}{\cdot}K^{-1}$ and 4.3 $J{\cdot}kg^{-1}{\cdot}K^{-1}$, respectively. This suggests that the current strategy of using transition metal Co to regulate the magnetic interactions in RCu_2-based compounds to achieve a large MCE under low magnetic fields is feasible. The observed results are attributed to significant alterations in the system and the local environment of R^{3+} upon Co doping, leading to a transition from antiferromagnetic (AFM) to ferromagnetic (FM) states. Notably, only a single peak in the magnetic entropy change is observed in the $-\Delta S_M(T)$ curve, indicating that the magnetic entropy of the compound is primarily contributed by the R^{3+} ions.

The $-\Delta S_M/\Delta\mu_0 H$ vs. $\mu_0 H$ curve was re-integrated to obtain magnetic field dependence curves of $-\Delta S_M$ at different temperatures, as shown in Figs. 10(a)–10(d). The results indicate that with increasing magnetic field, the $-\Delta S_M/\Delta\mu_0 H$ value for all compounds gradually increases, reaching a peak at 0.5 T. This suggests that $RCu_{2-x}Co_x$ (R = Er, Ho) compounds are more advantageous under low magnetic field conditions. Using a superconducting magnet as the magnetic field source would significantly increase the cost of the cooling system and add to its complexity. Furthermore, all compounds exhibit substantial $-\Delta S_M/\Delta\mu_0 H$ values within a 3–5 K range near the magnetic transition temperature, indicating that these compounds not only have a large $-\Delta S_M$ but also a relatively wide refrigeration temperature span.

Additionally, temperature-averaged $-\Delta S_M$ (TEC), the refrigerant capacity (RC), and the relative cooling power (RCP) are also key indicators used to evaluate the MCE, represented by[34–36]

$$\mathrm{TEC} = \frac{\int_{T_{\mathrm{mid}}-\frac{\Delta T_{\mathrm{lift}}}{2}}^{T_{\mathrm{mid}}+\frac{\Delta T_{\mathrm{lift}}}{2}} \Delta S_M(T)_{\Delta H,T}\,\mathrm{d}T}{\Delta T_{\mathrm{lift}}}, \tag{2}$$

$$\mathrm{RC} = \int_{T_{\mathrm{cold}}}^{T_{\mathrm{hot}}} |\Delta S_M(T)|\,\mathrm{d}T, \tag{3}$$

$$\mathrm{RCP} = |-\Delta S_M^{\max}| \times \delta T_{\mathrm{FWHM}}. \tag{4}$$

Here, ΔT_{lift} is the desired refrigeration temperature span, and T_{mid} is the temperature at which $-\Delta S_M^{\max}$ is achieved within the desired range. T_{hot} and T_{cold} correspond to the two temperatures at half of the $-\Delta S_M^{\max}$ value, and δT_{FWHM} is obtained from $T_{\mathrm{hot}} - T_{\mathrm{cold}}$. Figures 11(a)–11(d) summarize the magnetocaloric parameters of $RCu_{2-x}Co_x$ (R = Er, Ho) compounds under different magnetic fields. Under a varying magnetic field of 0–2 T, the TEC, RC, and RCP val-

ues are 12.9 J·kg^{-1}·K^{-1}, 145.1 J·kg^{-1}, and 189.9 J·kg^{-1} for $ErCu_{1.75}Co_{0.25}$; 9.5 J·kg^{-1}·K^{-1}, 109.3 J·kg^{-1}, and 136.7 J·kg^{-1} for $ErCu_{1.5}Co_{0.5}$; 9.1 J·kg^{-1}·K^{-1}, 138.1 J·kg^{-1}, and 177.9 J·kg^{-1} for $HoCu_{1.75}Co_{0.25}$; and 7.1 J·kg^{-1}·K^{-1}, 124.6 J·kg^{-1}, and 156.7 J·kg^{-1} for $HoCu_{1.5}Co_{0.5}$, respectively.

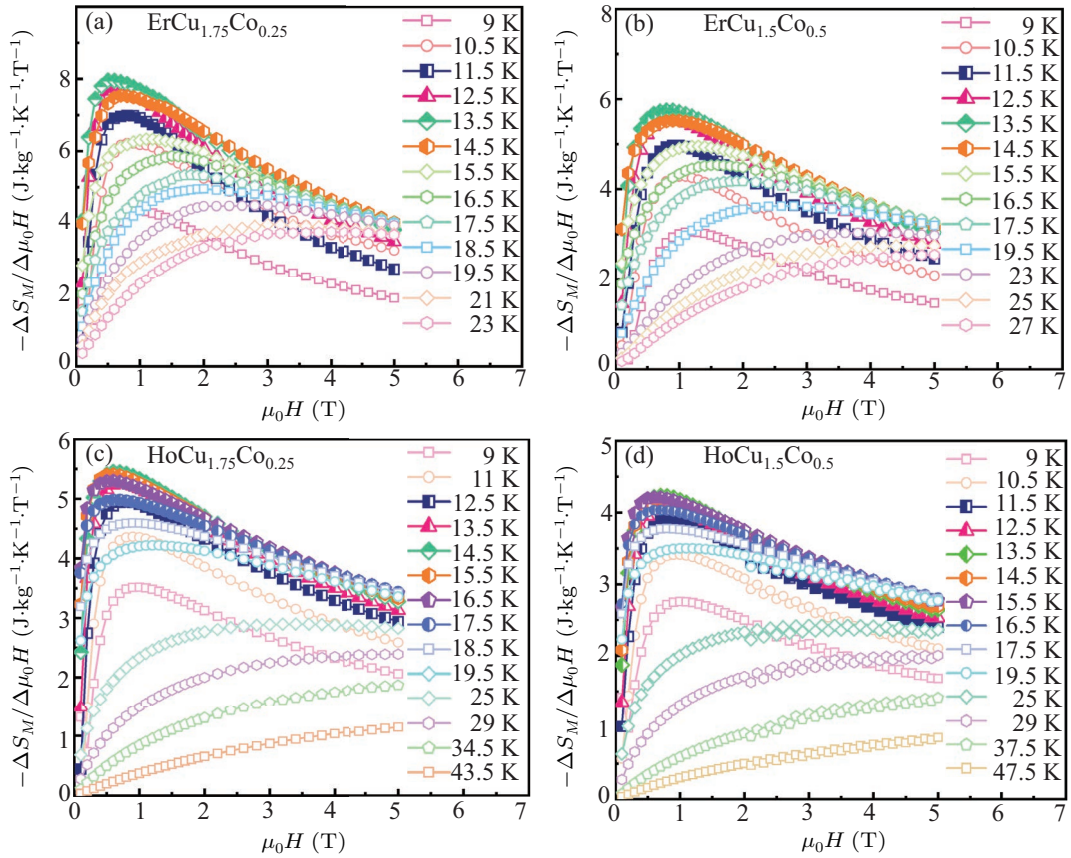


Fig. 10. (a)–(d) The $-\Delta S_M/\Delta\mu_0 H$ vs. $\mu_0 H$ under different magnetic fields. Here, $\mu_0 H_1 = \mu_0 H + \Delta\mu_0 H$ varies from $\mu_0 H$ to $\mu_0 H_2$, and $\mu_0 H$ is set to 0 T.

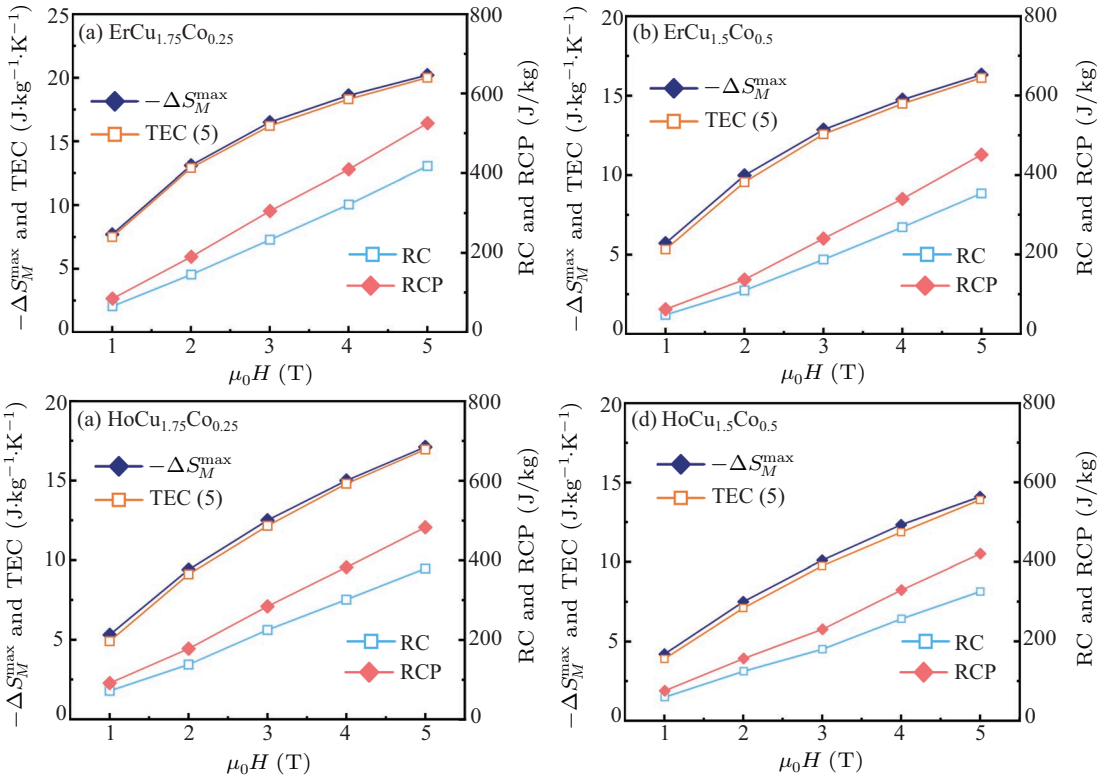


Fig. 11. (a)–(d) Maximum magnetic entropy change $-\Delta S_M^{max}$, TEC, RC, and RCP of $RCu_{2-x}Co_x$ compounds under different magnetic fields.

In the refrigeration process, magnetic refrigerants need to be combined with cold storage materials to fill the regenerator of the refrigerator, which is limited by its volume. A larger magnetocaloric effect within the available volume corresponds to higher cooling capacity and refrigeration power, which is crucial for the performance of MR systems. Therefore, attention to the volumetric magnetic entropy change ($-\Delta S_V$) of magnetic refrigerants is essential. Figure 12 compares the $-\Delta S_V$ of $R\mathrm{Cu}_{2-x}\mathrm{Co}_x$ (R = Er, Ho) compounds with other reported magnetic refrigerants under a 0–2 T magnetic field change. Near the hydrogen liquefaction temperature range, $\mathrm{ErCu}_{1.75}\mathrm{Co}_{0.25}$ exhibits superior performance compared to most materials, such as ErAl_2, $\mathrm{Er}_3\mathrm{Ni}_2$, and ErFeSi compounds.[37–39]

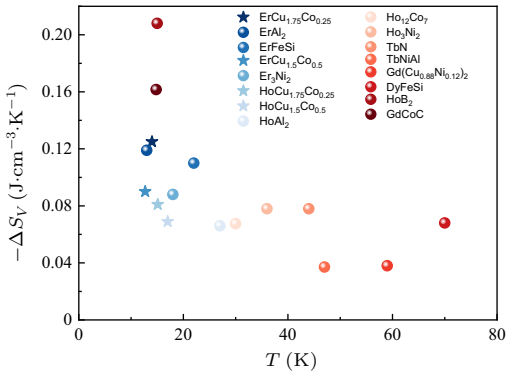


Fig. 12. Comparison of the volumetric magnetic entropy change of $R\mathrm{Cu}_{2-x}\mathrm{Co}_x$ compounds under a varying magnetic field of 0–2 T with other reported magnetocaloric materials in the liquid hydrogen temperature range. The volumetric magnetic entropy change was estimated based on the results reported in the following references: ErAl_2,[37] $\mathrm{Er}_3\mathrm{Ni}_2$,[38] ErFeSi,[39] HoAl_2,[40] $\mathrm{Ho}_{12}\mathrm{Co}_7$,[41] $\mathrm{Ho}_3\mathrm{Ni}_2$,[38] TbN,[42] TbNiAl,[43] $\mathrm{Gd}(\mathrm{Cu}_{0.88}\mathrm{Ni}_{0.12})_2$,[44] DyFeSi,[45] HoB_2,[46] and GdCoC.[47]

4. Conclusion

In summary, the magnetic interactions of $R\mathrm{Cu}_{2-x}\mathrm{Co}_x$ (R = Er, Ho) compounds transition to a ferromagnetic state upon doping with the transition metal Co, resulting in a significant enhancement of the MCE at low magnetic fields. The $\mathrm{ErCu}_{1.75}\mathrm{Co}_{0.25}$ compound exhibited a notable $-\Delta S_V$ of 0.12 J·cm^{-3}·K^{-1} under 0–2 T, surpassing many materials reported to date. Theoretical calculations elucidate the underlying mechanism of the magnetic variation. The reconstruction of the electronic structure and changes in the R^{3+} local environment are responsible for the emergence of the ferromagnetic phase. These findings suggest that Co-doped $R\mathrm{Cu}_2$ compounds hold potential for more energy-efficient and cost-effective magnetocaloric refrigeration systems, providing a viable path for advancing hydrogen liquefaction technologies. Moreover, the present results indicate that incorporating transition metal elements into rare-earth-based compounds to tune magnetic interactions and achieve tailored magnetic behaviors is a promising research direction.

Acknowledgments

This work was supported by the Light of the Soviet Area Innovation Leading Talent Program (Grant No. E23HB00101), the National Natural Science Foundation of China (Grant No. 52501262), and the Key Laboratory of Rare Earths, Chinese Academy of Sciences.

References

[1] Shirron P J, Kimball M O, Fixsen D J, Kogut A J, Li X Y and DiPirro M J 2012 *Cryogenics* **52** 140
[2] Shubham K, Arpit S, Ashish K, Adel Ben Y and Sheenam L 2023 *Appl. Energy* **334** 120670
[3] Nicita A, Maggio G, Andaloro A P F and Squadrito G 2020 *Int. J. Hydrogen Energy* **45** 11395
[4] Guillou F, Pathak A K, Paudyal D, Mudryk Y, Wilhelm F, Rogalev A and Pecharsky V K 2018 *Nat. Commun.* **9** 2925
[5] Xu J M, Yang F Y, Zhang Y K, Zhao X Y and Kong Z 2025 *Cryogenics* **154** 104266
[6] Na Y Z, Hao W X, Zhao X Y, Xie Y and Zhang Y K 2025 *Ceram. Int.* **51** 31140
[7] Song F Y, Liu X Y, Dong C, Zhou J, Shi X L, Han Y Y, Ling L S, Ren H F, Yuan S L, Wang S, Xiang J S, Sun P J and Tian Z M 2025 *Chin. Phys. Lett.* **42** 120706
[8] Chen W, Lin J L, Zhang Z Q and Li L W 2025 *J. Rare Earths*
[9] Tian L, Sun H B, Mo Z J, Gao X Q, Li Z X, Liu G D and Shen J 2025 *Int. J. Hydrogen Energy* **98** 1205
[10] Synoradzki K, Toliński T, Ul Ain Q, Matczak M, Romanova T and Kaczorowski D 2024 *J. Alloys Compd.* **1006** 176214
[11] Zhou X Y, Luo T, Wang C N and Fu H 2024 *J. Alloys Compd.* **976** 173264
[12] Chen W, Yin X Q, Lin J L, Hao W X and Zhang Y K 2024 *Ceram. Int.* **50** 32535
[13] Patino J C and de Oliveira N A 2024 *J. Alloys Compd.* **1003** 175685
[14] Zhang H, Wu Y Y, Long Y, Wang H S, Zhong K X, Hu F X, Sun J R and Shen B G 2014 *J. Appl. Phys.* **116** 213902
[15] Tian L, Xu B, Chen H, Mo Z J, Li Z X, Liu G D and Shen J 2023 *Sci. China Mater.* **66** 3984
[16] Chen J, Shen B G, Dong Q Y, Hu F X and Sun J R 2010 *Appl. Phys. Lett.* **96** 152501
[17] Zhang Y K, Zhu J, Li S, Zhang Z Q, Wang J and Ren Z M 2022 *Sci. China Mater.* **65** 1345
[18] Kotnana G, Sahu D P and Jammalamadaka S N 2017 *J. Alloys Compd.* **709** 410
[19] Li R K 2019 *Energy Technol.* **7** 1801070
[20] Hao J Z, Hu F X, Zhou H B, Liang W H and Yu Z B 2020 *Scr. Mater.* **186** 84
[21] Xie H C, Lv X D, Mo Z J, Gong J J, Gao X Q and Li Z X 2024 *J. Mater. Sci. Technol.* **193** 90
[22] Sugiyama K, Yamamoto T, Nakamura N, Thamizhavel A and Yoshii S 2003 *Physica B* **327** 423
[23] Sugiyama K, Yoshida Y, Aoki D, Settai R, Takeuchi T and Kindo K 1997 *Physica B* **230** 748
[24] Vargoz E, Link P and Jaccard D 1997 *Physica B* **230** 182
[25] Abliz M, Ahmet P, Aoki D, Kimura Y and Dahr S K 1997 *J. Phys. Soc. Jpn.* **66** 194
[26] Zheng X Q, Xu Z Y, Zhang B, Hu F X and Shen B G 2017 *J. Alloys Compd.* **712** 448
[27] Rajivgandhi R, Arout Chelvane J, Nigam A K, Malik S K and Nirmala R 2020 *J. Alloys Compd.* **815** 152659
[28] Kresse G and Joubert D 1999 *Phys. Rev. B* **59** 1758
[29] Blochl P E 1994 *Phys. Rev. B* **50** 17953
[30] Anisimov V I, Zaanen J and Andersen O K 1991 *Phys. Rev. B* **44** 943
[31] Wang V, Xu N, Liu J C, Tang G and Geng W T 2021 *Comput. Phys. Commun.* **267** 108033
[32] Banerjee B K 1964 *Phys. Lett.* **12** 16
[33] Franco V, Blázquez J S, Ipus J J and Law J Y 2018 *Prog. Mater. Sci.* **93** 112
[34] Griffith L D, Mudryk Y, Slaughter J and Pecharsky V K 2018 *J. Appl. Phys.* **123** 034902

[35] Gschneidner K A Jr and Pecharsky V K 2000 *Annu. Rev. Mater. Sci.* **30** 387
[36] Pecharsky V K and Tsokol A O 2005 *Rep. Prog. Phys.* **68** 1479
[37] Mahmud K, Gschneidner K A Jr and Pecharsky V K 2010 *J. Appl. Phys.* **107** 09A904
[38] Dong Q Y, Chen J, Shen J, Sun J R and Shen B G 2011 *Appl. Phys. Lett.* **99** 132504
[39] Zhang H, Shen B G, Xu Z Y, Shen J and Hu F X 2013 *Appl. Phys. Lett.* **102** 092401
[40] Hashimoto T, Kuzuhara T, Sahashi M, Inomata K, Tomokiyo A and Yayama H 1987 *J. Appl. Phys.* **62** 3873
[41] Zheng X Q, Shao X P, Chen J, Xu Z Y, Hu F X, Sun J R and Shen B G 2013 *Appl. Phys. Lett.* **99** 132504
[42] Takao Y A, Takashi N, Kengo S, Takatuki A and Hiroaki N 2004 *J. Alloys Compd.* **376** 1
[43] Singh N K, Suresh K G, Nirmala R, Nigam A K and Malik S K 2006 *J. Magn. Magn. Mater.* **302** 302
[44] Tian L, Mo Z J, Gong J J, Sun H B and Gao X Q 2024 *Mater. Res. Bull.* **177** 112828
[45] Zhang H, Sun Y J, Niu E, Yang L H, Shen J and Hu F X 2013 *Appl. Phys. Lett.* **103** 202412
[46] de Castro P B, Terashima K, Yamamoto T D, Hou Z F, Iwasaki S, Matsumoto R, Adachi S, Saito Y, Song P, Takeya H and Takano Y 2020 *NPG Asia Mater.* **12** 35
[47] Zhang Y K, Hao W X, Shen J, Mo Z J, Gottschall T and Li L W 2024 *Acta Mater.* **276** 120128